ICC2017: WS08-3rd International Workshop on Advanced PHY and MAC Technology for Super Dense Wireless Networks (CROWD-NET).

3D Channel Propagation in an Indoor Scenario with Tx Rooftop & Wall at 3.5 & 6 GHz

Yawei Yu*, Jianhua Zhang*, Xinzhuang Zhang*, Yu Zhang†
*Beijing University of Posts and Telecommunications, Beijing, China. † Qualcomm Inc, Beijing, China.
Email: {yyw,jhzhang,zxzhuang}@bupt.edu.cn, zhangyu@qti.qualcomm.com

***Abstract*—In this paper, we focus on the statistical characteristics of 3D channel propagation in indoor scenario with dense users. Measurements were performed at 3.5 and 6 GHz with 100 MHz by using an uniform cross-polarized rectangular transmitter (Tx) with 32 antennas and a cylindric cross-polarized receiver with 56 antennas. Placing the Tx at two different positions, against the wall which radiates signals forward and hanged on the rooftop which radiates signals downward, we repeat measurements and present comparative results of all 4 cases (2 frequency carriers $\times$ 2 Tx positions). Channel impulse response is obtained and key channel propagation parameters (angle information, 3D polarization components, etc) are extracted via the spatial-alternating generalized expectation-maximization algorithm. Results including power delay profile, delay spread, power angle spectrum, angle spread, cross polarization power ratios, channel capacity and capacity contribution ratios of eigenvalues, will provide further insights into 3D channel propagation.**

I. Introduction

With the rapid penetration of mobile-connected tablets like smart phones and virtual reality glasses, the mobile network connection speed is expected to increase more than three-fold by 2020 [1]. Key technologies are needed to meet this high capacity throughput requirements, especially for areas with dense users like enterprise cubicle indoor scenario. The most widely used technology Multiple-Input-Multiple-Output (MIMO), which adopts multiple antennas at both transmitter (Tx) and receiver (Rx), will provide significant spectrum efficiency improvement [2]. However, conventional MIMO only considers the azimuth domain, many channel measurements and modeling literatures ignore the elevation domain for simplicity [3]. Three dimensional (3D) MIMO, which further utilizes the additional elevation domain to meet higher network throughput demands [4], has attract people's wide attention [5].

Authors in [6] extended Clark's scattering model into 3D space for the first time and the impact of elevation domain on channel capacity is investigated [7]. Simulation work in [8] shows the promising potential of 3D MIMO in boosting spectrum efficiency. Field measurements further validate its superiority by harvesting obvious channel capacity gain [9]. Then theoretic analysis of 2D and 3D MIMO in terms of spatial correlation is presented [10]. Statistical results of 3D channel propagation in outdoor-to-indoor scenario provide us a better understanding of 3D channel propagation [11]. The obvious advantage of 3D MIMO in achieving better system performance makes it a key technology in future wireless networks [12].

In this paper, we concentrate on exploring the channel propagation statistic characteristics in enterprise cubicle indoor scenario with dense users. Measurements were conducted at 3.5 and 6 GHz with Tx placed against the rooftop and hanged on the rooftop. Comparative results are given, main contributions are listed:

- We conduct measurements at 4 different cases: 2 Tx positions (placed against the wall and hanged on the rooftop) $\times$ 2 frequency carriers (at 3.5 and 6 GHz). For each case, we calculate the channel impulse response (CIR) and extract key channel information including angles, 3D polarization components, etc.
- The obtained CIR enables us to further calculate power delay profile (PDP) and delay spread (DS) values for all measurement cases. More multipaths with different delays are observed for measurements at 3.5 GHz.
- The extracted 3D channel parameters enable us to present comparative results of power angle spectrum (PAS), angle spread (AS) and cross polarization power ratios (XPD). A larger angle dispersion is observed for Tx placed against the wall.
- Comparative system performances in terms of channel capacity are also investigated. For measurements at 3.5 GHz, a larger channel capacity is observed as compared to that at 6 GHz. Placing the Tx against the wall also lead to a larger channel capacity than that in Tx rooftop case. Further more, channel capacity contributions of eigenvalues for channel spatial correlation matrix are also presented.

The remainder of this paper is laid out as follows: In Section II, we give the description of the equipment and measurement scenario. Section III present the data post-processing method and Section IV illustrates comparative results. Conclusions are drawn in Section V.

II. Equipment and Scenario Description

A. Equipment Description

Measurements were done by utilizing the Elektrobit Propsound Sounder described in [13] to capture the real channel information. Full dimensional antenna arrays were equipped at both sides of the measurement link and the layout of Tx and Rx are illustrated in Fig. 1(a) and Fig. 1(b), respectively. For Rx, it is a dual-polarized omnidirectional array (ODA) consisting of 56 antenna elements with 8 adjacent sides and a

978-1-5090-1525-2/17/$31.00 ©2017 IEEE

top surface, while Tx is a dual-polarized uniform planar array (UPA) with 32 antenna elements. All array elements consisted of microstrip patches with 6 dB beamwidth of approximately 110^o in both the vertical and horizontal planes. The gain of each antenna element is 6 dBi, with an angle resolution of 2^o, which is limited by the sensors' distribution density in the anechoic chamber for antenna calibration. Table I specifies the configuration and angle range of the antenna arrays along with other measurement parameters. The angle ranges capture most of the propagation paths at both ends of the link, where paths with a delay interval larger than the delay resolution can be distinguished. All antennas were calibrated in an anechoic chamber.

TABLE I. Antenna configuration used in measurements

Parameter		Value	
Antenna type		ODA	UPA
Element number		56	32
Polarized		$\pm 45^o$	$\pm 45^o$
Distribution of antenna elements		cylinder	planar
Angle range	Azimuth	$-180^o \sim 180^o$	$-70^o \sim 70^o$
	Elevation	$-70^o \sim 90^o$	$-70^o \sim 70^o$
Carrier frequency		3.5 GHz & 6 GHz	
Bandwidth		100 MHz	
Transmit Power		32 dBm	

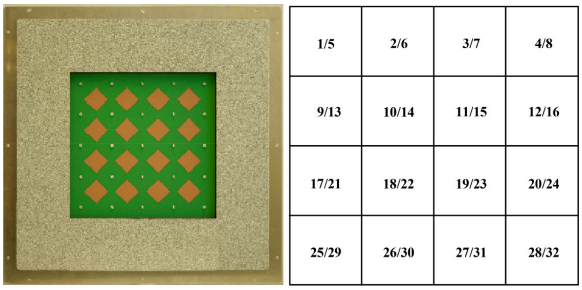

(a) Tx: 4×4 patches with each patch comprising a pair of cross-polarized antennas.

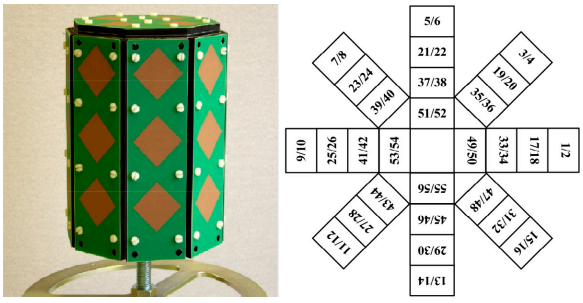

(b) Rx: 8 adjacent sides with 3 patches each, a top surface with 4 patches, each patch contains a pair of cross-polarized antennas.

Fig. 1: Antenna layouts used in the measurements.

B. Scenario Description

Measurements were done at a typical enterprise cubicle indoor scenario as shown in Fig. 2. The room is approximately

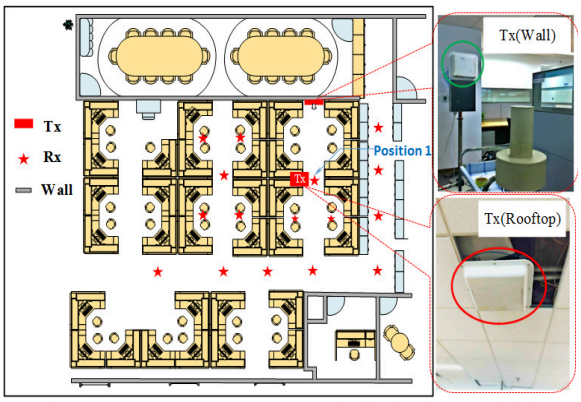

Fig. 2: Measurement scenario in indoor cubicle

22.5 × 7.5 × 3.5 m in length × width × height. There are lots of working compartments with 1.4 m width corridors. Rx was placed on a 1.8 m height trolley, and Tx was placed at two different positions, either placed against the wall to send signals forward or hanged on the rooftop which radiated signals downward. For each Tx position, 16 fixed locations including ones along the corridor and ones exactly in the working area would be collected. For each location, 500 samples were captured. We repeated the measurements at 3.5 and 6 GHz. Totally 16 (Rx locations)× 500 (samples) × 2 (Tx positions) × 2 (frequency carriers) samples were collected.

III. Data Post-processing

A. CIR Calculation

Signals propagating through the channel are collected by the Rx and stored in the sounder in binary bits with I data and Q data, thus the impulse response (IR) between antenna u in Rx and antenna s in Tx for path l, $h^{\mathrm{IR}}_{us,l}(t)$, can be calculated as $h^{\mathrm{IR}}_{us,l}(t) = I(t)+jQ(t)$. As it is the convolutional result of the system impulse response (SIR) $h^{\mathrm{SIR}}_{us,l}(t)$ and the CIR $h^{\mathrm{CIR}}_{us,l}(t)$, thus $h^{\mathrm{CIR}}_{us,l}(t)$ should be

$$h^{\mathrm{CIR}}_{us,l}(t) = \mathrm{IFFT}\left\{\frac{\mathrm{FFT}\left(h^{\mathrm{IR}}_{us,l}(t)\right)}{\mathrm{FFT}\left(h^{\mathrm{SIR}}_{us,l}(t)\right)}\right\}, \qquad (1)$$

where FFT and IFFT denote fast Fourier transform and inverse fast Fourier transform, respectively. Thus the $U \times S$ CIR matrix $\mathbf{H}$ is obtained, where U and S denote the total antenna number at Rx and Tx, respectively.

B. Key Channel Parameter Extraction

The collected CIRs were fed back to a high-resolution algorithm to estimate the channel parameters for each snapshot. Maximum likelihood estimation (MLE) provides an optimum unbiased estimation from a statistical perspective, however, it is computationally prohibitive due to the multidimensional searches required. Thus a low-complexity approximation of MLE, the spatial-alternating generalized expectation-maximization (SAGE) algorithm [14], has been proposed to extract the key channel parameters via the joint estimation. By substituting all possible values inside the antenna calibration file iteratively until the reconstructed signal best

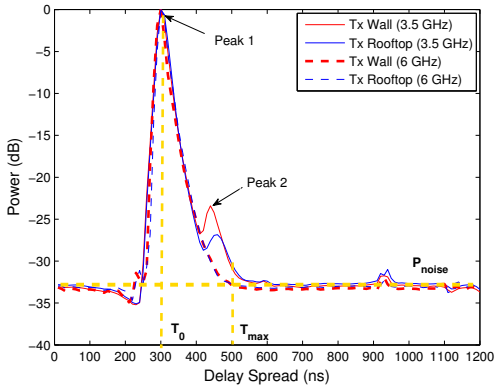

Fig. 3: PDP: Tx Rooftop & Wall at 3.5 & 6 GHz

TABLE II. Delay spread for all measurements

Tx Position		Rooftop		Wall	
Carrier Frequency		3.5 GHz	6 GHz	3.5 GHz	6 GHz
Delay Spread log 10([s])	μ	-7.08	-7.19	-7.05	-7.18
	σ	0.19	0.18	0.23	0.16
Mean Excess Delay (ns)		170.4	124.9	182.5	132.2
Max Excess Delay (ns)		372.3	278.6	387.4	291.2

fits the actual received one, we can extract the parameter set $\{\tau_l, \theta_l, \phi_l, \vartheta_l, \varphi_l, \alpha^l_{\mathrm{VV}}, \alpha^l_{\mathrm{HV}}, \alpha^l_{\mathrm{VH}}, \alpha^l_{\mathrm{HH}}\}$, which denote the delay, elevation angle of departure (EAoD), azimuth angle of departure (AAoD), elevation angle of arrival (EAoA), azimuth angle of arrival (AAoA), complex gains of vertical-to-vertical, horizontal-to-vertical, vertical-to-horizontal and horizontal-to-horizontal polarizations for path l, respectively.

IV. Statistical Results & Analysis

A. PDP & DS

As indicated in (1), the CIR for each Tx-Rx link would differ from each other due to antenna radiation gain and position differences. To present the overall characteristics, CIRs of all 32×56 links will be averaged to get the corresponding PDP. Paths with very small energy will get buried in the average calculation, the shape of the averaged PDP will be smoother than that of a single Tx-Rx link, only dominant peaks appear. In Fig. 3, PDPs for Rx at location 1 for all measurement cases are presented. Similar dynamical ranges of being 33 dB are observed for all 4 cases because the optical line-of-sight propagation distances from Tx rooftop/wall to Rx position 1 are approximately the same (1.4 m), no obvious pathloss difference between 3.5 and 6 GHz is expected due to the small propagation distance. Powers of multipaths decrease rapidly with delays, effective paths with delays within $[T_0, T_{\max}]$ are selected to make sure the minimum power of paths is 3 dB larger than noise level P_{noise}. Two obvious peaks arise for the measurements at 3.5 GHz, both for Tx placed against the wall and hanged on the rooftop cases. However, for measurements at 6 GHz, only one peak value is observed. As larger pathloss is experienced at higher frequency carrier, multipaths with large delay at 6 GHz would suffer serious pathloss and might not be received by the Rx. The overall delay spread values, mean excess delay and max excess delay are listed in Table. II. The comparative results indicate a better scattering at 3.5 GHz in terms of larger delay spread values.

B. Angle Distribution

1) PAS

Distribution of multipaths with different angles and powers can be reflected by PAS. Taking the Tx hanged on the rooftop and Rx located at position 1 as an example, PAS of all angles (AAoD, EAoD, AAoA, EAoA) at 3.5 and 6 GHz are illustrated in Fig. 4(a) and Fig. 4(b), respectively. As we can see, the angles of departure at 3.5 GHz distribute more widely than that of 6 GHz. For angle of arrival, a more dispersed angle distribution is observed as compared to that of departure.

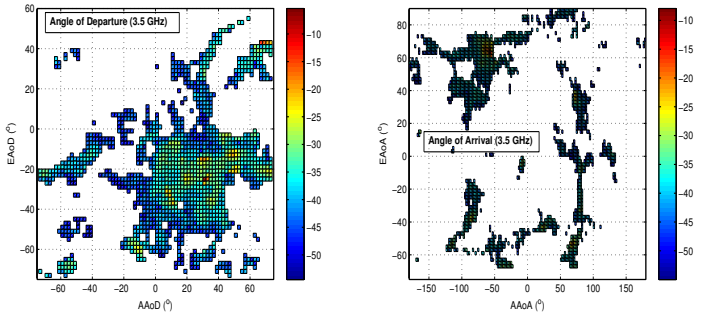

(a) PAS with Tx (rooftop)-Rx (position 1) at 3.5 GHz

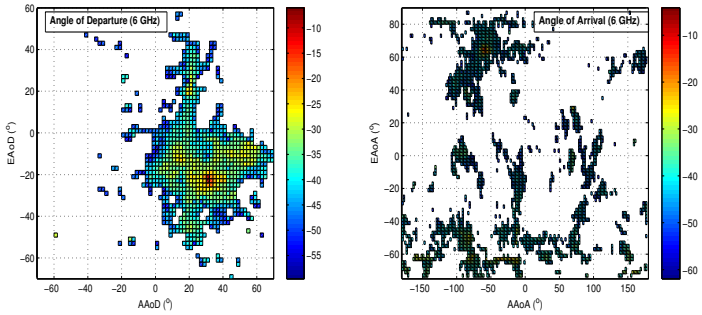

(b) PAS with Tx (rooftop)-Rx (position 1) at 6 GHz

Fig. 4: PAS with Tx (rooftop)-Rx (position 1) at 3.5 & 6 GHz

2) AS

Root mean square angle spread (rms AS) is regarded as one key parameter in measuring multipaths scattering and is defined [15]

$$\sigma_{\mathrm{AS}} = \sqrt{\frac{\sum_{l=1}^{L} (\theta_{l,\mu})^2 \cdot P_l}{\sum_{l=1}^{L} P_l}}, \tag{2}$$

where P_l is the power for path l, $\theta_{l,\mu}$ is defined as

$$\theta_{l,\mu} = \begin{cases} 2\pi + (\theta_l - \mu_\theta), & \text{if } (\theta_l - \mu_\theta) < -\pi \\ (\theta_l - \mu_\theta), & \text{if } |\theta_l - \mu_\theta| \le \pi \\ 2\pi - (\theta_l - \mu_\theta), & \text{if } (\theta_l - \mu_\theta) > \pi \end{cases} \tag{3}$$

μ_θ is defined as

$$\mu_\theta = \frac{\sum_{l=1}^{L} \theta_l \cdot P_l}{\sum_{l=1}^{L} P_l}. \tag{4}$$

and θ_l can be the AoA (or AoD, EOA, EOD) of path l.

TABLE III. Angle spread for all measurements

AS		Rooftop		Wall		InH (M.2135)
$\log_{10}(^\circ)$		3.5 GHz	6 GHz	3.5 GHz	6 GHz	LoS/NLoS
ESD	μ	1.52	1.24	1.36	1.22	-/-
	σ	0.23	0.21	0.20	0.19	- /-
ASD	μ	1.57	1.43	1.40	1.42	1.60/1.62
	σ	0.24	0.23	0.27	0.17	0.18/0.25
ESA	μ	1.35	1.35	1.52	1.38	-/-
	σ	0.20	0.16	0.22	0.16	-/-
ASA	μ	1.68	1.81	1.70	1.82	1.62/1.77
	σ	0.21	0.19	0.24	0.15	0.22/0.16

The mean μ and standard derivation σ of $\log_{10}(\sigma_{AS})$ for different Tx positions and frequency carriers are listed in Table. III. Comparing AS values at two different Tx positions, larger AS values at departure side are observed for Tx rooftop case for both two measurements at 3.5 and 6 GHz. By hanging the Tx high on the rooftop, signals are transmitted downwards and a larger area can be covered while signals transmitted at Tx wall case would be limited to a narrow directional space due to the dense office desks everywhere. For AS values of arrival (ESA, ASA), the multipaths are more dispersed when Tx is placed against the wall, signals experience richer scattering due to the denser scatters in the radiation direction. Comparing AS values at different frequency carriers, ESD, ESA and ASD at 3.5 GHz are larger than that of 6 GHz except ASA values. Higher frequency signals will be more of particle propagation which leads to a larger spread values within a narrow rich scattering environment and lower possibility to penetrate through the nearby glasses and wooden desks.

C. XPR

Based on the extracted 3D polarization components $\{\alpha_{VV}, \alpha_{\text{VH}}, \alpha_{\text{HV}}, \alpha_{\text{HH}}\}$, parameters including XPR, XPR from vertical to horizontal (XPR_{VH}) and XPR from horizontal to vertical (XPR_{HV}) can be calculated

$$\text{XPR} = \frac{\alpha_{\text{HH}}^2 + \alpha_{VV}^2}{\alpha_{\text{HV}}^2 + \alpha_{\text{VH}}^2}, \tag{5}$$

$$\text{XPR}_{\text{HV}} = \frac{\alpha_{\text{HH}}^2}{\alpha_{\text{HV}}^2}, \tag{6}$$

$$\text{XPR}_{\text{VH}} = \frac{\alpha_{VV}^2}{\alpha_{VH}^2}. \tag{7}$$

Their values for 4 measurement cases are listed in Table. IV. As we can see, XPR at Tx placed against the wall case is much larger than that of Tx rooftop case, which indicates a larger signal power conversion in 3D space for Tx rooftop case. With the increase of frequency carrier from 3.5 to 6 GHz, XPR values increase obviously.

TABLE IV. XPR for all measurements

Scenario	Rooftop		Wall		All	
Frequency	3.5 GHz	6 GHz	3.5 GHz	6 GHz	3.5 GHz	6 GHz
XPR[dB]	-0.82	-0.54	1.97	4.77	-0.58	2.11
XPR_{H2V}[dB]	-2.01	-1.35	1.98	5.20	-0.09	1.92
XPR_{H2V}[dB]	-0.01	-0.22	2.18	4.95	0.86	2.36

D. Channel Capacity

Being one of the important metrics for MIMO system performance, channel capacity will be calculated. To analyze the channel capacity of the wideband channel, the CIRs $\mathbf{H}(t,\tau)$ should be converted into the corresponding frequency impulse response $\mathbf{H}(t,f)$ by applying the Fourier transform. Assuming that the $\mathbf{H}(j,k)$ is the sample of $\mathbf{H}(t,f)$, then

$$\mathbf{H}(j,k) = \mathbf{H}(t,f)\,|_{t=j\cdot\Delta t, f=k\cdot\Delta f} = \mathbf{H}(j\cdot\Delta t, k\cdot\Delta f), \tag{8}$$

where Δt and Δf are the sampling intervals in time and frequency domains, respectively. In the absence of the channel state information at the transmitter, it is optimal to equally allocate power across all antennas. The channel capacity of the frequency-selective fading MIMO channel is given by [16]

$$C(t) = \frac{1}{B}\int_B \log_2 \det\left(I_U + \frac{\rho}{\beta^2 S}\mathbf{H}(t,f)\mathbf{H}^H(t,f)\right)df, \tag{9}$$

where ρ denotes the SNR and B is the bandwidth. For the discrete channel response $\mathbf{H}(j,k)$, an approximation is given by

$$C(j) \approx \frac{1}{K}\sum_{k=1}^{K}\log_2 \det\left(I_U + \frac{\rho}{\beta^2 S}\mathbf{H}(j,k)\mathbf{H}^H(j,k)\right), \tag{10}$$

where K is the number of frequency bins of the j^{th} time realization. β is a common normalization factor for all channel realizations to ensure that the average channel power gain is unitary as

$$\mathbb{E}\left\{\frac{1}{\beta}\|\mathbf{H}(j,k)\|_F^2\right\} = U\cdot S, \tag{11}$$

where $\|\|_F^2$ denotes the Frobenius norm.

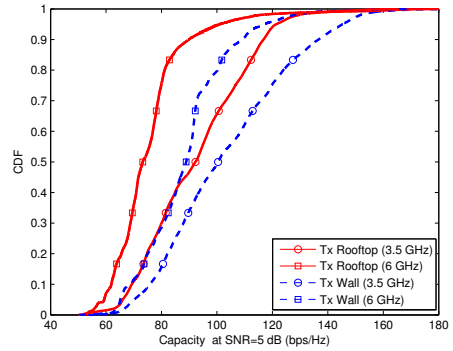

Fig. 5: Channel capacity of Tx rooftop & wall at 3.5 & 6 GHz

For the 56×32 MIMO system, comparative results of channel capacity for all 4 measurements at SNR=5 dB are illustrated in Fig. 5. Channel capacity values at 50% CDF point for Tx rooftop case at 3.5 GHz, Tx rooftop case at 6 GHz, Tx wall case at 3.5 GHz and Tx wall case at 6 GHz are 92.25 bps/Hz, 73.24 bps/Hz, 100.4 bps/Hz and 88.91 bps/Hz, respectively. Measurements at 3.5 GHz gain larger channel capacity than measurements at 6 GHz for both two Tx positions, which is consistent with the observation of larger DS, AS and XPR values at 3.5 GHz. By placing the Tx against the wall, a larger channel capacity is obtained.

E. Capacity Contribution Ratio of Eigenvalues

Eigenvalues of channel spatial correlation are calculated

1) Based on $\mathbf{H}(t,f)$ mentioned above, channel correlation matrix $\mathbf{R}$: $\mathbf{R} = \mathbf{H}(f)\mathbf{H}(f)^H$ (stationary environment)
2) Get the eigenvalues of $\mathbf{R}$: $\{\lambda_i, i = 1, 2, ..., \mathrm{r}(\mathbf{R})\} = \mathrm{Eigen}\{\mathbf{R}\}$

where $\mathrm{r}(\mathbf{R})$ is the rank of $\mathbf{R}$. Channel capacity contribution ratio of λ_i is defined

$$\gamma_i = \frac{C_i}{C}, \tag{12}$$

$$C = \sum_{i=1}^{\mathrm{r}(\mathbf{R})} \log_2\left(1 + \lambda_i \frac{\rho}{S}\right), \tag{13}$$

$$C_i = \log_2\left(1 + \lambda_i \frac{\rho}{S}\right). \tag{14}$$

In Fig. 6, Channel capacity contribution ratio of eigenvalue 1 (γ_1), total contribution ratio of eigenvalue 1 to 8 ($\sum_{i=1}^{8}\gamma_i$) and eigenvalue 1 to 16 ($(\sum_{i=1}^{16}\gamma_i)$) are illustrated. For i.i.d channel, the capacity contribution ratio of each eigenvalue for a 56×32 MIMO system should be 1/32, approximately 0.0313. For practical channel, the capacity contribution ratio of the largest eigenvalue is almost three times larger, being 0.0837, 0.075, 0.1035, 0.0881 for measurements with Tx rooftop at 3.5 GHz, Tx wall at 3.5 GHz, Tx rooftop at 6 GHz and Tx wall at 6 GHz, respectively. Larger capacity contribution values of eigenvalues for Tx rooftop case at 6 GHz indicates the existence of dominant eigenvalues.

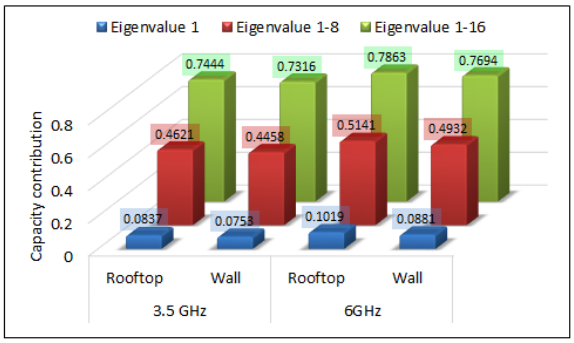

Fig. 6: Capacity contribution ratios of eigenvalues

V. Conclusion

In this paper, we provide comparative results including PDP, DS, PAS, AS, XPR, channel capacity and capacity contribution ratios of eigenvalues for measurements conducted in an indoor scenario under 4 cases: 2 Tx positions (against the wall and hanged on the rooftop) × 2 frequency carriers (3.5 and 6 GHz). Results show that more multipaths are observed for measurements at 3.5 GHz (PDP in Fig. 3), which leads to larger DS values. The intuitive PASs for Tx rooftop–Rx position 1 (see Fig. 2) show a much wider distribution of AAoD and EAoD at 3.5 GHz than that at 6 GHz. By hanging the Tx on the rooftop, larger AS values of departure (ESD, ASD) are observed. The Tx position has a great impact on XPR values, higher frequency carrier also lead to much larger XPR values. For the measurement conducted at 3.5 GHz with Tx placed against the wall case, we get the largest channel capacity. For the measurement conducted at 6 GHz with Tx hanged on the rooftop, larger capacity contribution ratios of eigenvalues indicates the higher spatial correlation in 3D channel propagation. Collectively, these comparative statistical results will contribute to a better understanding of 3D channel propagation.

VI. Acknowledgement

This research is supported in part by National Natural Science Foundation of China and project 'Ultra-dense network for 5G with the MTC application' with NO. 6141101115, and by 863 program under grant NO. 2014AA01A705, and by Qualcomm Incorporated.

References

[1] Cisco, "Cisco visual networking index: Global mobile data traffic forecast, 2015-2020," White Paper, Feb, 2016.
[2] G. J. Foschini and M. J. Gans, "On limits of wireless communications in a fading environment when using multiple antennas," *Wireless personal communications*, vol. 6, no. 3, pp. 311–335, 1998.
[3] M. Series, "Guidelines for evaluation of radio interface technologies for IMT-Advanced," *Report ITU*, pp. 2135–1, 2009.
[4] J. Zhang, C. Pan, F. Pei, G. Liu, and X. Cheng, "Three-dimensional fading channel models: A survey of elevation angle research," *Communications Magazine, IEEE*, vol. 52, no. 6, pp. 218–226, 2014.
[5] 3GPP TR 36.873 V.2, "Study on 3D channel model for LTE (Release 12)," Technical Report, 2014.
[6] T. Aulin, "A modified model for the fading signal at a mobile radio channel," *IEEE Transactions on Vehicular Technology*, vol. 28, no. 3, pp. 182–203, 1979.
[7] M. Shafi, M. Zhang, P. J. Smith, A. L. Moustakas, and A. F. Molisch, "The impact of elevation angle on MIMO capacity," in *2006 IEEE International Conference on Communications*, vol. 9, pp. 4155–4160, IEEE, 2006.
[8] Y.-H. Nam, B. L. Ng, K. Sayana, Y. Li, J. Zhang, Y. Kim, and J. Lee, "Full-dimension MIMO (FD-MIMO) for next generation cellular technology," *IEEE Communications Magazine*, vol. 51, no. 6, pp. 172–179, 2013.
[9] Y. Yu, J. Zhang, and M. Shafi, "3D vs. 2D channel capacity of outdoor to indoor scenarios derived from measurements in China and New Zealand," in *Signal Processing Conference (EUSIPCO), 2016 24th European*, pp. 1980–1984, IEEE, 2016.
[10] Y. Yu, P. J. Smith, P. A. Dmochowski, J. Zhang, and M. Shafi, "3D vs. 2D channel models: spatial correlation and channel capacity comparison and analysis (submitted)," in *2017 IEEE International Conference on Communications (ICC 2017)*, IEEE.
[11] Y. Yu, J. Zhang, M. Shafi, M. Zhang, and J. Mirza, "Statistical characteristics of measured 3-Dimensional MIMO channel for outdoor-to-indoor scenario in China and New Zealand," *Chinese Journal of Engineering*, vol. 2016, 2016.
[12] W. H. Chin, Z. Fan, and R. Haines, "Emerging technologies and research challenges for 5G wireless networks," *IEEE Wireless Communications*, vol. 21, no. 2, pp. 106–112, 2014.
[13] Y. Yu, J. Zhang, M. Shafi, P. A. Dmochowski, M. Zhang, and J. Mirza, "Measurements of 3D channel impulse response for outdoor-to-indoor scenario: Capacity predictions for different antenna arrays," in *Personal, Indoor, and Mobile Radio Communications (PIMRC)*, pp. 408–413, IEEE, 2015.
[14] B. H. Fleury, M. Tschudin, R. Heddergott, D. Dahlhaus, and K. I. Pedersen, "Channel parameter estimation in mobile radio environments using the SAGE algorithm," *IEEE Journal on selected areas in communications*, vol. 17, no. 3, pp. 434–450, 1999.
[15] 3GPP TR 25.996 V.9.0.0, "3rd generation partnership project; technical specification group radio access network; spatial channel model for multiple input multiple output (mimo) simulations (release 9)," Technical Report, 2009.
[16] D. P. Palomar, J. R. Fonollosa, and M. A. Lagunas, "Capacity results of spatially correlated frequency-selective MIMO channels in UMTS," in *Vehicular Technology Conference, 2001. VTC 2001 Fall. IEEE VTS 54th*, vol. 2, pp. 553–557, IEEE, 2001.